Title
Methane Storage: Molecular Mechanisms Underlying Room-Temperature Adsorption in Zn4O(BDC)3 (MOF-5)

Journal
Journal of Physical Chemistry C, 121(22)

ISSN
1932-7447

Authors
Tsivion, E
Head-Gordon, M

Publication Date
2017-06-08

DOI
10.1021/acs.jpcc.7b04246

Peer reviewed

Methane Storage: Molecular Mechanisms Underlying Room-Temperature adsorption in $Zn_4O(BDC)_3$ (MOF-5)

Ehud Tsivion[†, §] and Martin Head-Gordon[‡, §]

† Materials Sciences Division and ‡ Chemical Sciences Division, Lawrence Berkeley National Laboratory, Berkeley, California 94720, United States.

§ Department of Chemistry, University of California, Berkeley, California 94720, United States

* Email: mhg@cchem.berkeley.edu

Abstract

In this paper we study how the methane adsorption properties of the ionic MOF-5 are derived from the local structure of its coordinated metal-cluster. Density functional theory is used to study the adsorption process and identify the key interactions which drive it at ambient temperatures. A detailed adsorption model which represents the adsorption process is derived and used to extract thermodynamic properties from previously reported adsorption isotherms. We find that after adsorption of a single molecule to the face of the metal cluster, a nano-structured surface is formed which enables adsorption of additional of CH_4 molecules at reduced entropic penalty thanks to on-surface hopping motions and retention of significant translational freedom. Binding of the CH_4 molecules to the MOF is dominated by electrostatic interactions with negatively charged carboxylate groups, while CH_4-CH_4 dispersion interactions are important only at high pressures. Last, the MOF-specific adsorption model is compared against the single-site Langmuir model.

Introduction

As a transportation fuel, natural gas is a viable alternative to gasoline with several advantages such as low emissions and interchangeability with renewable biomethane.[1] Being composed mostly of methane (CH_4), natural gas in its standard state suffers from low energy density and needs to be compressed or liquefied in order to be used on-board passenger vehicles, limiting its operating range and requiring special, bulky, storage equipment. In principle, storage of natural gas by adsorption in a high surface area, nanoporous, material[2,3] is a promising alternative approach: the adsorbed gas takes a much smaller volume compared to its standard state, enabling storage at lower pressures with considerably less storage volume.

Due to their high surface area per unit volume and large pores, metal-organic frameworks (MOFs) are recognized as promising candidates for gas storage applications.[4–6] MOFs can also be post-synthetically modified to gain new functionalities that further "tailor" their properties.[7] To be able to design new CH_4 adsorbing MOFs, or any other porous material, it is important to have a detailed understanding of the atomistic factors that drive the adsorption process. In particular, identifying specific chemical or structural elements that govern optimal adsorption is of critical importance, as these could potentially be post-synthetically introduced, or alternatively, incorporated as a component in a specifically crafted adsorption system.

The $Zn_4O(BDC)_3$ framework (where BDC^{2-} = 1,4-benzenedicarboxylate), also known as MOF-5 or IRMOF-1, can be considered as a benchmark system for understanding gas-sorption processes in MOFs,[8–10] MOF chemistry[11,12] and CH_4 adsorption[13–15] in particular. As seen in Figure 1, MOF-5 has a cubic crystalline structure which consists of tetrahedral Zn_4O clusters coordinated by carboxylate-terminated BDC linkers.

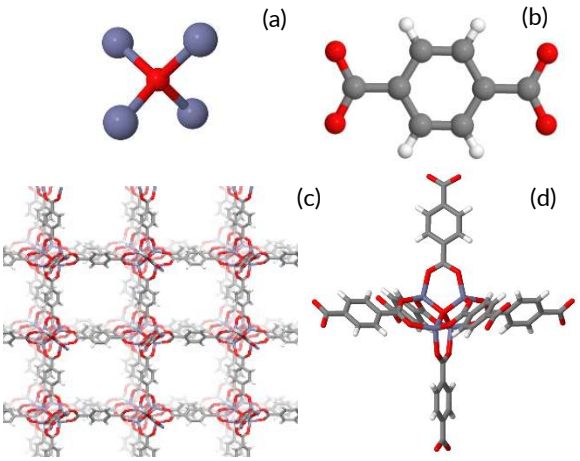

Figure 1. Structure of MOF-5. The Zn_4O metal clusters (a) are coordinated by six BDC linkers (b) and form the crystal structure (c). A close-up on a coordinated cluster is shown in panel (d).

Experimentally measured adsorption isotherms of CH_4 in MOF-5 show a good fit to a single-site Langmuir model, implying that adsorption can be reasonably described using

just one type of adsorption site,[16] as Langmuir theory suggests. However, this simple picture stands in contrast to previous adsorption studies of other gases in MOF-5, mostly hydrogen[17–20] as well as others,[21] which have suggested that several distinct adsorption sites exist, each with its own unique characteristics. Moreover, neutron diffraction experiments of MOF-5 have identified three different types of CH_4 adsorption sites,[22] directly implying that the single-site Langmuir behavior in MOF-5 masks more complex adsorption behavior.

To obtain a detailed understanding of the CH_4 adsorption process in MOF-5, all adsorption sites should be characterized in terms of location and binding energy. Moreover, to connect these properties to the thermal properties of enthalpy, entropy and free energy, a model which describes the adsorption process itself, in greater detail than the simple Langmuir model, is needed.

In this article we report the computational investigation of CH_4 adsorption in MOF-5. By integrating previously reported findings from neutron powder diffraction by Wu et al.,[22] gas-sorption measurements by Mason et. al.[16] with our own models and density functional theory (DFT) calculations, we are able to provide insights beyond the potential energy surface provided by DFT and report thermodynamic quantities and adsorption site occupancies. Whereas most MOF adsorption studies make use of force-field based simulations,[23] approaches based on DFT/cluster calculations have the advantage of providing a more accurate and detailed description of MOF-adsorbate interactions.[24] Nonetheless, the number of studies which connect site-interaction to experimental adsorption isotherms is very limited.[20,25,26] The approach taken here constitutes a methodology that permits tractable application of more accurate electronic structure methods, beyond the insights into the physical processes themselves.

Models, methods and computational details

The fundamental unit of interest in MOF-5 is the metal cluster and its coordinated linkers. The metal cluster, Zn_4O^{6+} in Figure 1 panel a, is tetrahedral in shape and each pair of its zinc atoms is coordinated by a carboxylate group that belong to the $C_8O_4H_4^{2-}$ linker (benzene-1,4-dicarboxylate or BDC^{2-} in Figure 1 panel b). Since four zinc ions form six unique zinc-pairs, the Zn_4O^{6+} tetrahedral cluster is coordinated by six linkers. Each BDC^{2-} linker contains two carboxylate groups and is coordinated to two metal clusters on each of his edges.

The local models used to study CH_4 adsorption are carved out of the crystal structure (Figure 2), and mimic the chemical environment corresponding to adsorption sites at or adjacent to the Zn_4O^{6+} cluster. Thus all local models retain the Zn_4O^{6+} cluster itself and truncate the crystal lattice at the linkers by removing distant carboxylate groups. Retained linkers that are relevant to adsorption are modeled by replacing BDC with $C_7O_2H_6^-$ (phenyl carboxylate). When the linker itself is not needed, it is further truncated by replacing the aromatic ring with a methyl group.

Model M1 (Figure 2) is used for studying adsorption on and near the face of the metal cluster ("cup structure"), by retaining the cluster itself and three coordinating linkers that together form a cup-like shape. The other three remote linkers are truncated by replacing their aromatic ring with a methyl group. Model M2 (Figure 2) is designed for studying adsorption on the top (vertex) of the metal cluster ("top-site"). It retains the metal cluster and the three relevant linkers and truncates the others with methyl groups. It is assumed that CH_4 adsorption on the cup structure does not affect adsorption in the top-site and vice versa. The model geometries are derived from the crystal structure provided by the Cambridge Crystallographic Data Center,[27] CSD entry SAHYIK01.[28,29]. The structure of the MOF is assumed to remain fixed regardless of the amount of CH_4 adsorbed, supported by the findings of Wu el al.[22] In the Supplementary Information is shown that the calculated adsorption energy values are robust with respect to small changes in the crystal structure, by separately evaluating them using a slightly different crystal structure[30] obtained at 300 K.

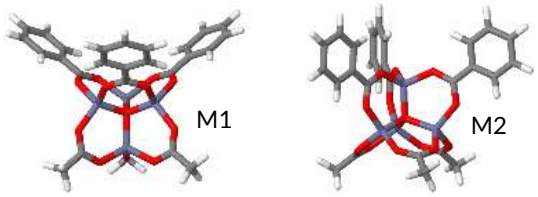

Figure 2. Models for MOF-5 and adsorption sites. M1 is used for studying CH_4 adsorption on the "cup structure" and M2 is used for the "top-site".

Geometry optimization of the adsorbed molecules is performed while constraining the geometry of the binding site atoms to their crystalline positions, optimizing the locations of the hydrogen atoms and the adsorbed CH_4 molecules. All calculations are carried using the meta-GGA B97M-V density functional,[31] which utilizes the VV10 non-local correlation functional for its treatment of dispersion interactions.[32] The 6-31G* basis set[33] is used for geometry optimization while interaction energies are calculated using the def2-QZVP[34] basis with no counterpoise correction. Validation of the accuracy of the 6-31G* basis-set for geometry is found in the Supplementary Information. Previous CH_4 adsorption studies indicate that the basis set superposition error is typically less than 0.3 kJ/mol for the def2-QZVP basis. The B97M-V/def2-QZVP combination is expected to yield a statistical error of 0.6 kJ/mol, as benchmarked against the A24 data set for noncovalent interactions,[35] also, a recent benchmark by Herbert and coworkers on intermolecular interactions involving ions demonstrated that B97M-V performs very well for anion-neutral dimers, cation-neutral

dimers and ion pairs.[36] The optimized geometries are verified to be minima on the potential energy surface (PES) using partial hessian analysis for the atoms of the adsorbed molecules. All calculations were performed using the Q-Chem quantum chemistry package.[37]

Results

Adsorption on the cup structure. The face of the Zn_4O cluster is surrounded by linkers that form a cup structure. It is found that there are three types of CH_4 adsorption sites in the cup structure. Their calculated positions are shown in Figure 3 panels (a) to (d).

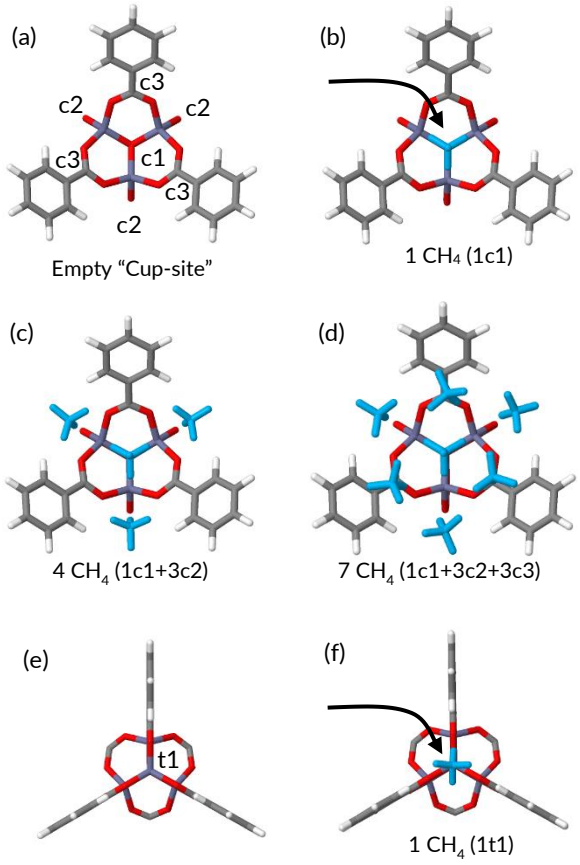

Figure 3. Adsorption of CH_4 on the cup structure panels (a) to (d) and on the on the t1 site ("top site") panels (e) and (f). CH_4 are blue-colored. The occupancy of the site is given in parentheses.

Table 1. Adsorption energies for the four different types of adsorption sites on the cup-site. The number in parentheses next to the c3 sites indicates the number of adjacent occupied c2 sites.

	c1	c2	c3(0)	t1	c3(1)	c3(2)
ΔE_{ads} [kJ/mol]	−18.9	−12.1	−9.0	−11.7	−10.1	−12.0

The first site, denoted by c1, is positioned above the center of the cluster. With an adsorption energy of −18.9 kJ/mol, it is the strongest adsorbing site. The second type of site, denoted by c2, are positioned between the two aromatic rings. The adsorption energy is −12.1 kJ/mol, weaker by ~7 kJ/mol than the c1 site. The third type of site, denoted by c3, are positioned above the aromatic rings and are shared with the adjacent metal cluster. The c3 adsorption energy is relatively weak (−9.0 kJ/mol); however, this binding energy can increase to −12.1 kJ/mol if the two adjacent c2 sites are occupied. The cup-structure can therefore adsorb up to seven CH_4 molecules when completely saturated: 1c1+3c2+3c3 (Figure 3 (d)).

Cup-structure adsorption is found to be a sequential reaction: for a CH_4 molecule to adsorb on c2 or c3, c1 must first be occupied. This is a feature of the PES: unless c1 is already occupied, adsorption on c2 or c3 is not a minimum of the PES and the molecules "relax" into c1 during geometry optimization. Interestingly, adsorption on c3 is not completely conditional, but highly dependent, on the presence of adsorbed molecules in c2. Given that c1 is occupied, adsorption of a CH_4 molecule on c3 exists as a minimum on the PES with a relatively weak ΔE_{ads} of −9.0 kJ/mol which is insufficient for significant occupancy at room-temperature. However, if a neighboring c2 is occupied, ΔE_{ads} is increased by −1.1 kJ/mol. If two neighboring c2's are occupied ΔE_{ads} is increased by −3.1. To distinguish the various adsorption configurations for c3, the number of adjacent adsorbed CH_4 molecules is noted in parentheses, e.g. c3(1) for a single neighboring CH_4 molecule in a c2 site, and c3(2) for two.

Since c3 is shared between two metal-clusters, it is surrounded by four c2 sites or a maximum of four CH_4 molecules such that a c3(4) configuration exists. Based on the c3(0) to c3(2) trend, we expect ΔE_{ads} for c3(4) to be in between −14 to −15 kJ/mol. However, the c3(4) configuration involves a large number of simultaneously adsorbed molecules, so that at ambient temperature, c3(4) can only be significantly occupied at very high pressures, near saturation of the MOF.

Adsorption on the t1 site. The t1 site is located on a vertex of the ZnO_4 cluster, above a zinc atom, as shown in Figure 3 panels (e) and (f). The adsorption interaction in t1 is −11.7 kJ/mol close to that of c2 and is expected to increase at higher pressures due to the proximity of the c2's to t1. However, neutron powder diffraction experiments do not indicate that CH_4 molecules adsorb on t1,[22] even when the adjacent c2 sites are fully populated.

Since no evidence for a barrier to adsorption on t1 is found, it can be argued that adsorption on the t1 site has a large enough negative entropy change so that it is thermodynamically unfavorable at ambient temperature.

Other adsorption sites. Other CH_4 adsorption sites can potentially be found anywhere inside the MOF when temperature is sufficiently low (such as the center of the pore[22]). However, due to the weakness of these residual interactions, these sites cannot contribute to adsorption at ambient conditions and are therefore not further considered.

Electronic basis for the attraction of CH_4 to MOF-5. A key question in understanding adsorption in MOF-5 is understanding the mechanism by which the presence of the Zn_4O^{6+} clusters induces a strong attractive force to CH_4. When complexed to the Zn_4O^{6+} cluster the negative charge on the carboxylate group on the BDC^{2-} linker is increased due to polarization of the aromatic ring by the positive zinc ions. In benzoic acid, Figure 4(a), the oxygen atom that is covalently bound to a hydrogen atom has a natural charge, given by natural population anaylsis,[38] of −0.63e. Its conjugate base, Figure 4(b), is negatively charged and both oxygen atoms carry a larger charge of −0.75e. For MOF-5, (c), the charge on the oxygen is −0.83e, which indicates an increased, though not complete, ionic character.

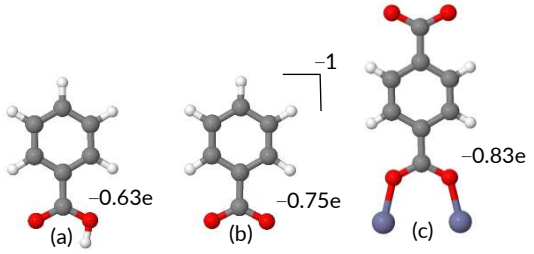

Figure 4. Natural charge on the oxygen atom: Phenyl carboxylic acid (a) its conjugate base (b) for MOF-5 (c).

The energy of adsorption of CH_4 is therefore expected to be related to the degree of exposure to the negatively charged oxygen atoms of the carboxylate groups. As shown in Figure 5, the CH_4 in c1 is exposed to six oxygens and has a strong ΔE_{ads} of −18.9 kJ/mol. At c2 CH_4 is exposed to a two oxygens and has a smaller ΔE_{ads} of −12.1 kJ/mol. At t1 CH_4 is exposed to three oxygens and is attracted by −11.7 kJ/mol, slightly weaker than at c2 and possibly due to steric repulsion from its more confined surroundings.

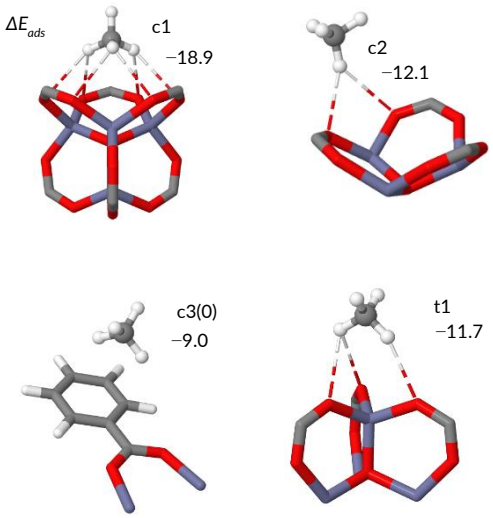

Figure 5. Methane adsorption sites in MOF-5 and related ΔE_{ads} values in kJ/mol. Interactions between the methane hydrogens and carboxylate oxygens are indicated by dashed lines.

Importance of CH_4-CH_4 and dispersion interactions. The maximum interaction energy of between two CH_4 molecules in the gas phase is about −2.1 kJ/mol at a carbon to carbon distance of 3.6 - 3.9 Å, as calculated by Tsuzuki et al.[39] In the cup structure, the distances between CH_4 molecules in c1 and c2 is almost optimal at about 3.8 Å and between c2 and c3 at about 4.0 Å, implying that CH_4-CH_4 interactions also contribute for ΔE_{ads}.

We evaluate CH_4-CH_4 interactions explicitly by calculating interaction energies of adsorbed CH_4 molecules in absence of the MOF. The interaction between c1 and c2 contributes about −1 kJ/mol, which is relatively small with respect to the overall c2 interaction of −12.1 kJ/mol. However, for the c3 sites these interactions play a more significant role, where CH_4 molecules adsorbed on the nearest c2 contribute about −3 kJ/mol, increasing the interaction from −9 to −12 kJ/mol, as already mentioned. Adsorption to c3 sites is therefore shows positive cooperativity, in which molecules at c2 induce extra attraction at c3. Other than CH_4-CH_4 interactions, significant interaction at c3 also originates from the interaction of the CH_4 molecule and the aromatic ring, which is dominated by dispersion interactions.

Given the exponential dependence of the adsorption reaction constant on the free energy of adsorption, the −1 to −3 kJ/mol dispersion related increase is essential for c3 to play a significant role in the adsorption reaction.

Analysis of charge transfer, polarization and frozen interactions. Energy decomposition analysis of the bonding energy at the various sites is shown in Table 2.

Table 2. Energy decomposition analysis for interactions of adsorbed CH_4 molecules.

	c1	c2	c3(2)	t1
Frozen	−12.1	−7.5	−7.1	−7.1
Polarization	−1.7	−1.1	−1.1	−1.2
Charge-transfer	−5.0	−3.5	−2.9	−3.4
Total	−18.9	−12.1	−12.0	−11.7

For all sites, the most dominant interactions are “Frozen” which indicates strong non-induced electrostatic interactions and/or dispersive attraction. Polarization, or induced-electrostatic, interactions do not seem to play a major role and are usually in between −2 to −1 kJ/mol. Charge transfer interactions are between −5 to −3 kJ/mol and are particularly strong for adsorption at c1, due the large number of O–H interactions.

Although the Zn ions at the vertices of the Zn_4O^{6+} tetrahedron are known to function as Lewis acids,[40] by using charge transfer analysis,[41] we found no evidence of significant charge-transfer interactions between the CH_4 and Zn. Methane is simply too poor a Lewis base.

Adsorption model. To pursue further insight into the adsorption process beyond electronic interactions, a statistical model of adsorption is devised. The basic building blocks of the model are “adsorption configurations” which represent different arrangements of

up to seven adsorbed CH_4 molecules in the cup structure. In principle, the model should include all possible adsorption configurations in a "cluster-expansion" which includes all possible configurations that involve a single molecule, two molecules and so forth, up to a maximum of seven. Although inclusion of all possible configurations should ideally increase the model's accuracy, it also increases the number of parameters. Instead, following the "*Occam's razor*" principle, we develop a minimalist model which retains the most important configurations and requires only a small number of approximated or fitted parameters. The minimalist approach should be more robust (or stable) with respect to any parameter fitting, as will later be required.

The following assumptions are made in the selection of retained configurations: (1) a molecule cannot occupy a c2 site unless c1 is also occupied. (2) a molecule cannot occupy a c3 site unless the two adjacent c2 sites are also occupied, i.e., only the c3(2) configurations are included. Since certain configurations that are less likely at high temperatures, such as a c3 occupied with no occupation of c2 (i.e. c3(0)), are excluded, the model's quality and predictive capabilities are expected to degrade at lower temperatures. (3) The free (non-adsorbed) CH_4 molecules present in the pore volume do not significantly interact with the adsorbed ones.

The adsorption model is manifested by the adsorption polynomial, Q which represents the relative weight of each possible adsorption configuration. The full form of Q is long and as is shown in full in the supporting information. An abbreviated form of Q which involves only the first terms is:

$$Q = \sum_i p^i \sum_{j=1}^{i} \sigma_j K_j = 1 + K_{c1}p + K_{c1}K_{c2}p^2 + K_{c1}2K_{c2}p^2 + \cdots \quad (1)$$

The p^i term is the pressure of CH_4, raised to i^{th} power, where i is the number of adsorbed molecules for a given configuration. The K_j terms are the equilibrium constants for configuration j and are evaluated using the well-known relation $K_j = \exp(-\Delta G_j/RT)$ where ΔG_j is the free energy of adsorption. If configuration K_j is degenerate, K_j is multiplied by the number of possible combinations σ_j. The average number of CH_4 molecules that occupy the site at a given pressure, $\theta(p)$, is given by:

$$\theta(p) = Q^{-1} \sum_i i \cdot p^i \sum_{j=1}^{i} \sigma_j K_j \quad (2)$$

this expression becomes the well-known Langmuir equation for the case of a single adsorption site. Unlike the Langmuir model, the value of $\theta(p)$ can be as high as the maximal number of adsorbed molecules, which is seven in this model. We clarify that the equilibrium constant K_j represent the ratio of occupied to vacant sites of type j. Thus, a positive value of ΔG_j implies that number of occupied sites of type j is smaller than the number vacant sites at any given pressure.

The adsorption isotherm, which indicates the amount of adsorbed methane at a given pressure, $n_{ads}(p)$, is given by:

$$n_{ads}(p) = \theta_{c1}(p) \cdot n_{1CH4} + \theta_{c2}(p) \cdot n_{1CH4} + \theta_{c3}(p) \cdot \frac{n_{1CH4}}{2} \quad (3)$$

Here n_{1CH4} is the amount of methane, in v[STP]/v, that is adsorbed in the MOF if a single site fully occupied. The contribution of the c3 sites, $\theta_{c3}(p)$, is halved since they are shared with adjacent metal clusters.

The value of n_{1CH4} is derived from the crystal structure, since that the concentration of a single adsorbed CH_4 is the same as the concentration of its adsorption site. For MOF-5, the value of n_{1CH4} is 70.38 v[STP]/v.

Derivation of thermodynamic quantities. For isolated molecules in the gas phase, thermodynamic properties, such as entropy and enthalpy are usually calculated using quantum chemistry in the harmonic approximation. This approach is inappropriate for physisorption systems for two reasons: (1) As a result of the weak interactions, the system deviates strongly from harmonicity and (2) as will become evident later, the adsorbed CH_4 molecules may retain some fraction of their gas-phase translational and rotational degrees of freedom, but it is hard to quantify how much freedom is lost in the adsorption process. Since translations and rotations have the largest contribution to the entropy, the most difficult challenge is to reliably evaluate the adsorption entropy, ΔS_{ads}, which in this context is the thermodynamic force that resists adhesion/localization of the CH_4 molecule to the MOF.

To avoid the above issue, some key thermodynamic quantities are derived by fitting the adsorption model to the experimental CH_4 adsorption isotherms of MOF-5 reported by Mason et al.[16] In the fitting process, optimal values for the equilibrium constant K_j for the different adsorption configurations are found. The free energy of adsorption, ΔG_{ads}, are obtained from the K_j's through the well-known relation: $K_j = exp(-\Delta G_{ads}/RT)$. The fitting procedure is numerically stable and different optimization algorithms provided similar free energies.

The free energy of adsorption has two components, given by the well-known relation $\Delta G_{ads} = \Delta H_{ads} - T\Delta S_{ads}$. To avoid any further parameter fitting, the adsorption enthalpies, ΔH_{ads}, are evaluated as:

$$\Delta H_{ads} = \Delta E_{ads} - \mathrm{R} \cdot \mathrm{T} + \Delta \mathrm{U}_{vib} \quad (4)$$

The electronic adsorption energy (ΔE_{ads}) is obtained from the DFT calculations. The $-\mathrm{R} \cdot \mathrm{T}$ term corresponds to the contribution of the volume term $-\mathrm{p} \cdot \mathrm{V}$ and ΔU_{vib}, the adsorption-related internal energy of vibration, is approximated to be −2.5 kJ/mol at ambient temperature, assuming a formation of a single vibration of about 150 cm^{-1} upon adsorption to the MOF surface.

Once ΔH_{ads} is evaluated, the adsorption entropies are obtained by: $\Delta S_{ads} = (\Delta G_{ads} - \Delta H_{ads})/T$. Since the contribution of internal vibrations ΔU_{vib} is only estimated, the extracted ΔS_{ads} may be slightly contaminated by errors

in ΔU_{vib}. Although this assessment of the thermodynamic quantities is a rough estimate, the final results agree well with experimental observations as well as qualitative understanding, and are without doubt far superior to direct calculations in the harmonic approximation.

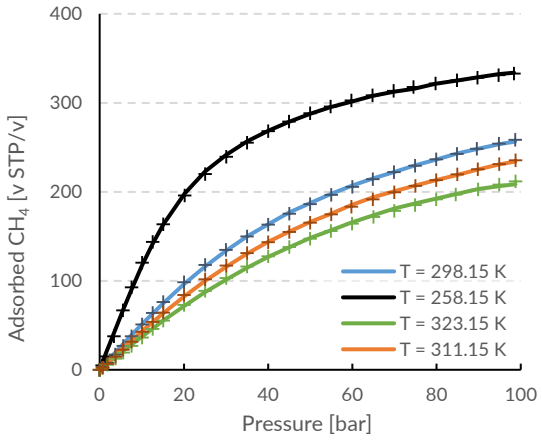

Figure 6. MOF-5 adsorption isotherms at various temperatures. Experimental[16] and theoretical-model curves are marked by solid lines and crosses respectively.

Table 3. Model-fitted entropy and free energies of adsorption at T = 298.15 K. ΔS_{ads}/R is unit-less, ΔH_{ads} and ΔG_{ads} are given in kJ/mol.

Site	ΔH_{ads}	ΔS_{ads}/R	ΔG_{ads}
c1	−18.8	−10.5	7.1
c2	−12.1	−8.9	9.9
c3(2)	−12.0	−10.0	12.8

The results for the thermodynamic quantities and adsorption isotherms, as obtained by fitting the model to the experimental adsorption isotherms[16] are given in Table 3 and Figure 6 respectively. The resulting model is a very good fit to the experimental isotherm. When compared against fitting a single-site Langmuir model, the fit error for our model is smaller by 86% to 91% when evaluated as the Euclidean norm of the difference between experimental and fitted model values. Since the model is designed for ambient temperatures, the error for fitting for 258.15K is almost four times larger than for the higher-temperature results, which indicates that certain degrees of freedom that are important at lower temperatures are missing in order to provide a high-accuracy fitting.

The c1 site has a large negative ΔS_{ads} of −10.5R which correlates with the strong adsorption enthalpy. The c2 sites, have a relatively smaller ΔS_{ads} of −8.9R, implying that molecules adsorbed on these sites have a higher degree of motional freedom. Interestingly, in-spite of having a similar adsorption enthalpy as c2, the c3(2) sites have a more negative ΔS_{ads} of −10.0R.

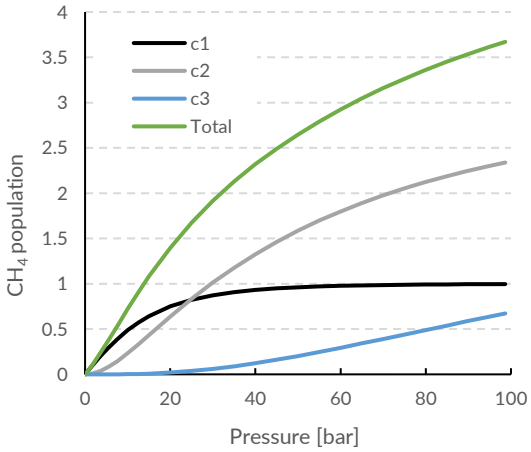

Figure 7. Occupation of the adsorption sites at 298.15 K. Total is evaluated at c1 + c2 + c3/2. The maximum population for c1 is 1CH_4 and 3CH_4 for both c2 and c3 respectively.

To validate the robustness of the model with respect to adsorption on the c3 sites, we've also used a smaller version of the model without any c3 sites. The smaller model yielded very similar results at pressures of up to 35 bar, where participation of c3 is expected by the larger model to be small. Further details are found in the Supplementary Information.

Occupation of the sites. The number of adsorbed CH_4 molecules on each of the sites (site occupancy) predicted by the model, is shown in Figure 7. The strongly adsorbing c1 site is the first to be occupied and reaches occupancy of 0.5 at about 11 bar. The c2 sites are second to populate and reach occupation of 1.5 (half of their maximum 3) at about 47 bar. Due their larger number, the population of the c2 sites surpasses the occupation of c1 at 25 bar and continues to increase such that at 100 bar they reach occupancy of 2.3 molecules. The rise in the population of the c2 sites, even at relatively low pressures, is due to the quick occupation of the strongly interacting c1 sites, which is required for adsorption in c2's. Since occupation of the c3 requires occupation of the c2 sites, the c3 population begins to rise slowly at about 30 bar, and continues to rise at a slow rate such that even at 100 bar they are far from saturation.

Usable capacity. The MOF's ability to deliver stored methane to an internal combustion engine is defined as the amount of methane stored at maximum pressure, which is typically taken as 35 or 65 bar, minus the amount stored at minimal pressure of 5.8 bar, which is usually assumed (for comparative reasons) as the minimal pressure required for gas to flow from the fuel tank to the combustion engine. Therefore, to maximize usable capacity, a minimal amount of CH_4 should be stored at lower pressures and maximal amount should be stored at maximal pressure. At 5.8 bar only the c1 sites are significantly occupied by about 0.3 molecules, a relatively small amount that does not hinder capacity due to over-adsorption. At 35 and 65 bar, the c1 site is almost completely saturated, such that the methane content of the MOF is limited by the occupancy of the c2's

which is 1.2 and 1.9 molecules at 35 and 65 bar respectively. The c2 sites are therefore far from saturation at higher pressures and any decrease in their free energy of adsorption would result in a significant increase in usable capacity.

At ambient conditions, the c3 sites do not contribute to usable capacity for maximum 35 bar and contribute marginally at 65 bar.

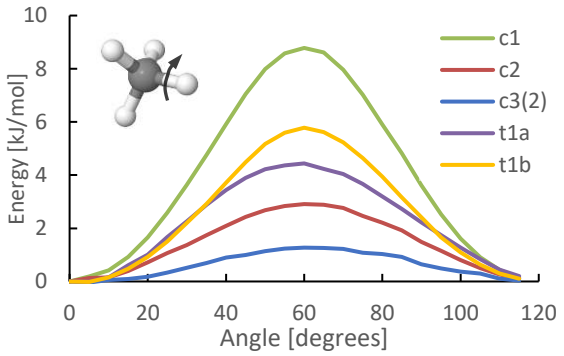

Figure 8. Barriers for rotations along the C--H bonds of the adsorbed methane molecule. Two barriers are identified for the t1 site.

Barriers for rotation. To further investigate the rotational degrees of freedom of the adsorbed molecules, the barriers for rotation around the C—H bonds of the adsorbed CH_4 molecules are calculated using with the def2-TZVP basis set[42], the results shown in Figure 8.

The barrier of rotation for c1 is very high, about 8.8 kJ/mol, meaning that methane adsorbed in c1 is not expected to have significant rotational freedom. Perhaps the main reason for this high rotational barrier is because the adsorbed CH_4 molecule at c1 is held by six H—O interactions (Figure 5) which yields preferred positions ("anchors") for three of its hydrogen atoms.

Adsorption on the c2 sites is characterized by a smaller rotational barrier of about 2.8 kJ/mol, which is slightly higher than the average kinetic energy at 298.15 K of $RT = 2.48$ kJ/mol. Thus, a CH_4 molecule in c2 is close to being free to rotate. The CH_4 molecule is anchored only by a double H—O interaction; its barrier is about a third of the barrier for c1 which is anchored by three. The rotational barrier appears to be roughly proportional to the number of anchored hydrogen atoms: each anchored hydrogen atom contributes slightly less than 3 kJ/mol to the barrier.

For the c3 sites, the adsorbed CH_4 molecule is held mostly by weak intermolecular dispersion forces, which are less orientation dependent than the H—O interactions in c1 and c2. Accordingly, the orientational preference of CH_4 molecules in c3 is very small and the rotational barrier is only 1.3 kJ/mol which is much smaller than the available thermal energy. Molecules adsorbed in c3 are therefore free to rotate.

CH_4 molecules adsorbed in t1 are anchored by two hydrogen atoms, however, one of the hydrogen atoms is held by only a single H—O interaction. Accordingly, the rotational barriers in t1 are relatively high: 4.5 and 5.8 kJ/mol.

The low rotational barriers for the c2 and c3 sites, as well as the high barrier for c1, are in agreement with neutron diffraction experiments which indicate that CD_4 molecules adsorbed in c2 and c3 sites are orientationally disordered, while CD_4 in c1 is clearly oriented.[22]

Diffusion mechanisms. At room temperature, thermally related properties, such as entropy and internal vibrations, play a decisive role in the adsorption process. Since methane's internal degrees of freedom are only marginally altered upon adsorption onto the MOF, the main sources of changes in entropy upon adsorption (ΔS_{ads}) are the inter-molecular degrees of freedom: translations and rotations. Upon adsorption, strong localization or restriction of rotational and translational motions are expected to result in large negative ΔS_{ads} values as well as an increase in internal energy, due to the formation of internal vibrations associated with these restricted motions.

Values obtained for ΔS_{ads} by fitting to the model were shown above at Table 3. The large value for ΔS_{ads} for c1 of $-10.5R$ correlates well with its strong binding energy of −18.9 kJ/mol. Also, the high barriers for rotation are expected to restrict the motions of the adsorbed molecule at c1 and thus a large negative value of ΔS_{ads} is expected.

The large difference in ΔS_{ads} between c2 and c3(2) is peculiar at first glance. Although molecules in c2 and c3(2) are attracted by similar ΔE_{ads} of about −12 kJ/mol, the rotational barriers are considerably lower for c3(2) which is expected to rotate freely. Hence the magnitude of ΔS_{ads} should be somewhat smaller for c3 than c2. However, the ΔS_{ads} value for c2 is only $-8.9R$, much smaller than $-10.0R$ for c3(2), which implies that the entropy of a CH_4 molecule at c2 is higher, i.e. it is less confined, than at c3(2). Since rotational barriers cannot account for these difference, we infer that translational motions of the adsorbed molecules are the determining factor for the large difference in ΔS_{ads}.

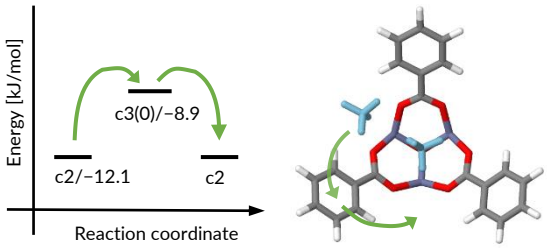

Figure 9. The c2-c3(0)-c2 "springboard" mechanism.

To rationalize the higher entropy at c2 vs c3, we propose two mechanisms which allow for more translational freedom, or local diffusion, of molecules adsorbed at c2. The first mechanism, which we shall call the "springboard" mechanism, is relevant up to about 70 bar when the c2 sites are populated by one or two CH_4 molecules. A CH_4 molecule in c2 uses an empty c3(0) site, which is only 3.2 kJ/mol higher in energy, as a short lived intermediate

product or “springboard” to jump into an adjacent empty c2. The molecules adsorbed in c2 are therefore able to diffuse in the cup-site, jumping from one c2 site to the other, retaining more of their gas phase translational degrees of freedom.

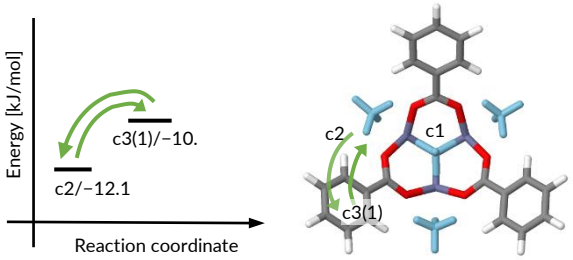

Figure 10. The c2-c3(1)-c2 “wall flip” mechanism.

Even when all the c2 sites are occupied, an adsorbed CH_4 molecules in c2 can still experience large-amplitude motions through the “wall flip” mechanism, where molecule adsorbed at c2 jumps to an adjacent c3(1) site, only 2 kJ/mol higher in energy, however, since the next c2 is occupied, the molecule flips back into its original location at c2. Due to the low barrier for this reaction, it is expected to be very fast and frequent.

These hopping mechanisms provides an explanation for the elevated ΔS_{ads} values for occupation of the c3 sites, which are expected to be occupied mostly at higher pressures. Since hopping into a filled site is sterically prohibited, as the cup-site is occupied with additional CH_4 molecules, hopping becomes less probable and the translational entropy of the adsorbed CH_4 is reduced. In other words, molecules adsorbed at the cup structure at higher cup structure occupations are expected to have larger ΔS_{ads} values due to a reduction in their translational motions as a result of increased packing.

In-spite of having approximately similar ΔE_{ads} as for c3(2) and c2, the t1 sites do not appear in neutron diffraction experiments to be occupied. This can be explained by an elevated ΔS_{ads} that is related to adsorption on t1. Rotational motions in t1 are restricted by barriers of 4.5 and 5.8 kJ/mol which are somewhat higher than for c2. Furthermore, a CH_4 molecule adsorbed at t1 is tightly packed, confined by three aromatic rings which restrict its motions. It is therefore likely that adsorption on t1 is thermodynamically disfavored at ambient temperatures due to barriers for rotation and spatial confinement.

Discussion

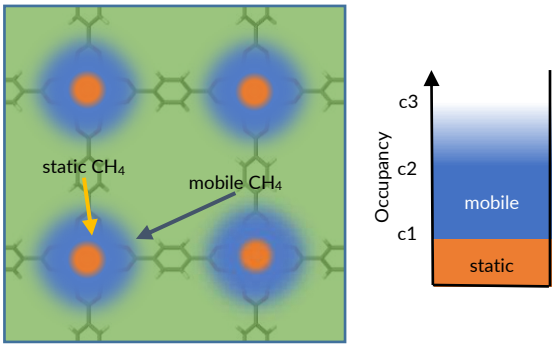

Figure 11. Qualitative depiction of adsorbed CH_4 at the cup structure at ambient temperatures and pressure of about 65 bar. Orange, blue and green represent static, mobile and gaseous CH_4 molecules.

An alternative way of contextualizing the results, rather than adsorption enthalpies, is depicted in Figure 11. The molecules adsorbed in c1 are strongly confined, lack translational and rotational motions and therefore can be considered as relatively static. Molecules adsorbed on the c2/c3 sites are freer to translate, or hop, inside the cup structure and can be considered as being relatively more mobile. If the c2/c3 sites become occupied by a large number of molecules (at very high pressures) the translational motions in the cup structure are increasingly hindered and the c2/c3 adsorbates become less mobile. However, this immobilization process is thermodynamically unfavorable at ambient temperatures and is expected to be observed only at very high pressures, possibly above 300 bar, as a rough estimate.

Limitations of the Langmuir model. As mentioned in the introduction, the Langmuir model provides a good fit to experimental adsorption data for CH_4 adsorption in MOF-5, suggesting that only a single type of adsorption site is involved in the adsorption reaction. It is therefore interesting to analyze how such a simple model provides a reasonable approximation to the complicated behavior described above.

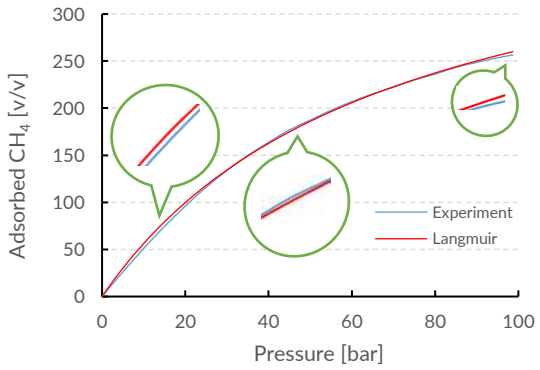

Figure 12. Langmuir model fit for adsorption isotherm of CH_4 in MOF-5 at T= 298.15K as reported by Mason at el.[16]

The green shapes point to the areas in which the fitted Langmuir curve deviates from experiment.

The Langmuir-like behavior of the experimental isotherm is a result of overlapping adsorption processes, in which partial occupation of a particular site is continuously followed by the partial occupation of another, with significant overlap between the two. For instance, the population of sites c1 and c2 increases simultaneously between 5 and 40 bar, and the population of the c2 and c3 sites each increase continuously above 40 bar.

The overlapping nature of the transition between occupation of different classes of adsorption sites, makes identifying them more subtle than obvious. However, lacking the necessary degrees of freedom, the Langmuir model deviates from the experimental CH_4 uptake within three distinct domains (Figure 12), each of which characterized by adsorption on a particular type of sites: the first domain is characterized by adsorption to c1, the second to c2 and the third marks increased adsorption to c3. The deviation from the ideal Langmuir model is reproduced in all measurements reported by Mason et al. at various temperatures[16] (see section S5 in the Supplementary Information), which also demonstrates of their robustness.

Furthermore, it is not the chemistry behind the Langmuir model which provides a good fit to the experimental isotherm. Rather, it is the functional form associated with the model, while the model itself does not faithfully represent the underlying adsorption process, as already discussed in detail. The functional form of the Langmuir model is:

$$\theta(p) = \frac{1}{1 + K_{ads} \cdot p} \cdot n_{sat} \qquad (5)$$

A usual fit procedure involves the fitting of the adsorption equilibrium parameter, K_{ads}, and the saturation capacity n_{sat}. The fitted parameters for CH_4 adsorption in MOF-5 at 298.15 K are K_{ads}= 0.015 bar^{-1} and n_{sat} = 439.34 [v/v]. Assuming that at room temperature, adsorption occurs only on the surface of the metal cluster, the physical interpretation of these numbers is that each cup structure holds a maximum of (non-physical) 6.2 CH_4 molecules at saturation, compared to actual maximum of 5.5 (= 7 – 3/2) since c3 is shared with an adjacent cluster). The value of K_{ads} corresponds to a ΔG_{ads} of 10.25 kJ/mol that is close to the value associated with adsorption to c2 (9.9 kJ/mol) and can be considered as an average value over the c1, c2 and the c3 sites. If the Langmuir functional form is to be imposed with a physically-acceptable value of n_{sat}, it would not be able to provide a fit with of quantitative agreement quality. By contrast, our model imposed a structurally derived value for n_{1CH4} of 70.38 v[STP]/v and then fitted the equilibrium constants for the three sites we identified.

Conclusion

In conclusion, the electronic interactions which drive the adsorption of methane in MOF-5 appear to originate mostly from the negatively charged carboxylate groups and to a lesser extent, dispersion interactions. Zinc ions do not participate by directly interacting with the CH_4 molecules by themselves, other than via dispersion, and charge-compensation.

Apart from the attractive forces already mentioned, adsorption on MOF-5 is also strongly affected by the (methane-dependent) nano-structured surface formed on the faces of its metal-cluster, which permits some adsorbed CH_4 molecules to retain a significant degree of translational motion while being adsorbed. This important property alleviates the entropic tendency to resist adsorption to the surface and also compensates for weaker adsorption energy. While the importance of hopping mechanisms for diffusion of guest species in zeolites[43–45] and MOFs,[46–48] we have identified the important contribution of these hopping steps to the stabilize the c2 adsorbed state. We note that the suggested mechanisms are purely intra-stitial and do not result in MOF-wide diffusion of CH_4.

From the perspective of the application of MOF-5 for methane storage, the usable capacity of MOF-5 is limited by the relatively small occupation of the c2 sites at higher pressures. Any increase in the affinity of the c2 sites for CH_4, or alternatively, any reduction of the entropy penalty that is associated with them, could significantly improve usable capacity. Since CH_4 adsorption on c2 sites is strongly dependent on the extent of negative charge carried by the carboxylate groups, increasing their negative charge could possibly increase CH_4 uptake. We've tested several modifications to MOF-5, such as linker-modifications or ZnO_4 cluster modifications by trans-metalation,[11,40] but were not not able to find a viable strategy for increasing the affinity of the carboxylate groups. We have also tested hypothetical models of Mg-MOF-5 where Zn is replaced by "harder" Mg ions, but we also find that the adsorption energies does not seem to change significantly as the partial charge of the carboxylate groups remains approximately the same. Thus postsynthetic modifcations, as we have recently analyzed in detail elsewhere,[49] may be the most promising avenue for enhanced methane storage in MOF-5.

Acknowledgment

We would like to thank Narbe Mardirossian, Daniel S. Levine, Jarad A. Mason and Jeffrey R. Long for useful discussions and advice. The authors gratefully acknowledge research support from the U.S. Department of Energy, Office of Energy Efficiency and Renewable Energy, Fuel Cell Technologies Office, under Contract DE-AC02-05CH11231, with additional support from the U.S. National Science Foundation under grant number CHE-1363342.

References

(1) Alternative Fuels Data Center: Natural Gas http://www.afdc.energy.gov/fuels/natural_gas.html (accessed Dec 17, 2015).

(2) Matranga, K. R.; Myers, A. L.; Glandt, E. D. Storage of Natural Gas by Adsorption on Activated Carbon. *Chem. Eng. Sci.* **1992**, *47* (7), 1569–1579.

(3) Makal, T. A.; Li, J.-R.; Lu, W.; Zhou, H.-C. Methane Storage in Advanced Porous Materials. *Chem. Soc. Rev.* **2012**, *41* (23), 7761–7779.

(4) Murray, L. J.; Dincă, M.; Long, J. R. Hydrogen Storage in Metal–organic Frameworks. *Chem. Soc. Rev.* **2009**, *38* (5), 1294.

(5) Czaja, A. U.; Trukhan, N.; Müller, U. Industrial Applications of Metal–organic Frameworks. *Chem. Soc. Rev.* **2009**, *38* (5), 1284–1293.

(6) He, Y.; Zhou, W.; Qian, G.; Chen, B. Methane Storage in Metal–organic Frameworks. *Chem. Soc. Rev.* **2014**, *43* (16), 5657–5678.

(7) Evans, J. D.; Sumby, C. J.; Doonan, C. J. Post-Synthetic Metalation of Metal–organic Frameworks. *Chem. Soc. Rev.* **2014**, *43* (16), 5933–5951.

(8) Rowsell, J. L. C.; Spencer, E. C.; Eckert, J.; Howard, J. A. K.; Yaghi, O. M. Gas Adsorption Sites in a Large-Pore Metal-Organic Framework. *Science* **2005**, *309* (5739), 1350–1354.

(9) Ford, D. C.; Dubbeldam, D.; Snurr, R. Q.; Künzel, V.; Wehring, M.; Stallmach, F.; Kärger, J.; Müller, U. Self-Diffusion of Chain Molecules in the Metal–Organic Framework IRMOF-1: Simulation and Experiment. *J. Phys. Chem. Lett.* **2012**, *3* (7), 930–933.

(10) Höft, N.; Horbach, J. Condensation of Methane in the Metal–Organic Framework IRMOF-1: Evidence for Two Critical Points. *J. Am. Chem. Soc.* **2015**, *137* (32), 10199–10204.

(11) Bellarosa, L.; Brozek, C. K.; García-Melchor, M.; Dincă, M.; López, N. When the Solvent Locks the Cage: Theoretical Insight into the Transmetalation of MOF-5 Lattices and Its Kinetic Limitations. *Chem. Mater.* **2015**, *27* (9), 3422–3429.

(12) Brozek, C. K.; Michaelis, V. K.; Ong, T.-C.; Bellarosa, L.; López, N.; Griffin, R. G.; Dincă, M. Dynamic DMF Binding in MOF-5 Enables the Formation of Metastable Cobalt-Substituted MOF-5 Analogues. *ACS Cent. Sci.* **2015**, *1* (5), 252–260.

(13) Brand, S. K.; Colón, Y. J.; Getman, R. B.; Snurr, R. Q. Design Strategies for Metal Alkoxide Functionalized Metal–organic Frameworks for Ambient Temperature Hydrogen Storage. *Microporous Mesoporous Mater.* **2013**, *171*, 103–109.

(14) Babarao, R.; Hu, Z.; Jiang, J.; Chempath, S.; Sandler, S. I. Storage and Separation of CO2 and CH4 in Silicalite, C168 Schwarzite, and IRMOF-1: A Comparative Study from Monte Carlo Simulation. *Langmuir* **2007**, *23* (2), 659–666.

(15) Zhou, W.; Wu, H.; Hartman, M. R.; Yildirim, T. Hydrogen and Methane Adsorption in Metal−Organic Frameworks: A High-Pressure Volumetric Study. *J. Phys. Chem. C* **2007**, *111* (44), 16131–16137.

(16) Mason, J. A.; Veenstra, M.; Long, J. R. Evaluating Metal–organic Frameworks for Natural Gas Storage. *Chem. Sci.* **2013**, *5* (1), 32–51.

(17) Sagara, T.; Klassen, J.; Ganz, E. Computational Study of Hydrogen Binding by Metal-Organic Framework-5. *J. Chem. Phys.* **2004**, *121* (24), 12543–12547.

(18) Mueller, T.; Ceder, G. A Density Functional Theory Study of Hydrogen Adsorption in MOF-5. *J. Phys. Chem. B* **2005**, *109* (38), 17974–17983.

(19) Bordiga, S.; Vitillo, J. G.; Ricchiardi, G.; Regli, L.; Cocina, D.; Zecchina, A.; Arstad, B.; Bjørgen, M.; Hafizovic, J.; Lillerud, K. P. Interaction of Hydrogen with MOF-5. *J. Phys. Chem. B* **2005**, *109* (39), 18237–18242.

(20) Sillar, K.; Hofmann, A.; Sauer, J. Ab Initio Study of Hydrogen Adsorption in MOF-5. *J. Am. Chem. Soc.* **2009**, *131* (11), 4143–4150.

(21) Dubbeldam, D.; Frost, H.; Walton, K. S.; Snurr, R. Q. Molecular Simulation of Adsorption Sites of Light Gases in the Metal-Organic Framework IRMOF-1. *Fluid Phase Equilibria* **2007**, *261* (1–2), 152–161.

(22) Wu, H.; Zhou, W.; Yildirim, T. Methane Sorption in Nanoporous Metal−Organic Frameworks and First-Order Phase Transition of Confined Methane. *J. Phys. Chem. C* **2009**, *113* (7), 3029–3035.

(23) Fang, H.; Demir, H.; Kamakoti, P.; Sholl, D. S. Recent Developments in First-Principles Force Fields for Molecules in Nanoporous Materials. *J. Mater. Chem. A* **2013**, *2* (2), 274–291.

(24) Odoh, S. O.; Cramer, C. J.; Truhlar, D. G.; Gagliardi, L. Quantum-Chemical Characterization of the Properties and Reactivities of Metal–Organic Frameworks. *Chem. Rev.* **2015**, *115* (12), 6051–6111.

(25) Chen, L.; Grajciar, L.; Nachtigall, P.; Düren, T. Accurate Prediction of Methane Adsorption in a Metal–Organic Framework with Unsaturated Metal Sites by Direct Implementation of an Ab Initio Derived Potential Energy Surface in GCMC Simulation. *J. Phys. Chem. C* **2011**, *115* (46), 23074–23080.

(26) Sillar, K.; Sauer, J. Ab Initio Prediction of Adsorption Isotherms for Small Molecules in Metal–Organic Frameworks: The Effect of Lateral Interactions for Methane/CPO-27-Mg. *J. Am. Chem. Soc.* **2012**, *134* (44), 18354–18365.

(27) Allen, F. H. The Cambridge Structural Database: A Quarter of a Million Crystal Structures and Rising. *Acta Crystallogr. B* **2002**, *58* (3), 380–388.

(28) Eddaoudi, M.; Li, H.; Reineke, T.; Fehr, M.; Kelley, D.; Groy, T. L.; Yaghi, O. M. Design and Synthesis of Metal-Carboxylate Frameworks with Permanent Microporosity. *Top. Catal.* **1999**, *9* (1–2), 105–111.

(29) Li, H.; Eddaoudi, M.; O'Keeffe, M.; Yaghi, O. M. Design and Synthesis of an Exceptionally Stable

and Highly Porous Metal-Organic Framework. *Nature* **1999**, *402* (6759), 276–279.

(30) Lock, N.; Wu, Y.; Christensen, M.; Cameron, L. J.; Peterson, V. K.; Bridgeman, A. J.; Kepert, C. J.; Iversen, B. B. Elucidating Negative Thermal Expansion in MOF-5. *J. Phys. Chem. C* **2010**, *114* (39), 16181–16186.

(31) Mardirossian, N.; Head-Gordon, M. Mapping the Genome of Meta-Generalized Gradient Approximation Density Functionals: The Search for B97M-V. *J. Chem. Phys.* **2015**, *142* (7), 74111.

(32) Vydrov, O. A.; Voorhis, T. V. Nonlocal van Der Waals Density Functional: The Simpler the Better. *J. Chem. Phys.* **2010**, *133* (24), 244103.

(33) Binkley, J. S.; Pople, J. A.; Hehre, W. J. Self-Consistent Molecular Orbital Methods. 21. Small Split-Valence Basis Sets for First-Row Elements. *J. Am. Chem. Soc.* **1980**, *102* (3), 939–947.

(34) Weigend, F.; Furche, F.; Ahlrichs, R. Gaussian Basis Sets of Quadruple Zeta Valence Quality for Atoms H–Kr. *J. Chem. Phys.* **2003**, *119* (24), 12753–12762.

(35) Řezáč, J.; Hobza, P. Describing Noncovalent Interactions beyond the Common Approximations: How Accurate Is the "Gold Standard," CCSD (T) at the Complete Basis Set Limit? *J. Chem. Theory Comput.* **2013**, *9* (5), 2151–2155.

(36) Lao, K. U.; Schäffer, R.; Jansen, G.; Herbert, J. M. Accurate Description of Intermolecular Interactions Involving Ions Using Symmetry-Adapted Perturbation Theory. *J. Chem. Theory Comput.* **2015**, *11* (6), 2473–2486.

(37) Shao, Y.; Gan, Z.; Epifanovsky, E.; Gilbert, A. T. B.; Wormit, M.; Kussmann, J.; Lange, A. W.; Behn, A.; Deng, J.; Feng, X.; Ghosh, D.; Goldey, M.; Horn, P. R.; Jacobson, L. D.; Kaliman, I.; Khaliullin, R. Z.; Kuś, T.; Landau, A.; Liu, J.; Proynov, E. I.; Rhee, Y. M.; Richard, R. M.; Rohrdanz, M. A.; Steele, R. P.; Sundstrom, E. J.; Woodcock, H. L.; Zimmerman, P. M.; Zuev, D.; Albrecht, B.; Alguire, E.; Austin, B.; Beran, G. J. O.; Bernard, Y. A.; Berquist, E.; Brandhorst, K.; Bravaya, K. B.; Brown, S. T.; Casanova, D.; Chang, C.-M.; Chen, Y.; Chien, S. H.; Closser, K. D.; Crittenden, D. L.; Diedenhofen, M.; DiStasio, R. A.; Do, H.; Dutoi, A. D.; Edgar, R. G.; Fatehi, S.; Fusti-Molnar, L.; Ghysels, A.; Golubeva-Zadorozhnaya, A.; Gomes, J.; Hanson-Heine, M. W. D.; Harbach, P. H. P.; Hauser, A. W.; Hohenstein, E. G.; Holden, Z. C.; Jagau, T.-C.; Ji, H.; Kaduk, B.; Khistyaev, K.; Kim, J.; Kim, J.; King, R. A.; Klunzinger, P.; Kosenkov, D.; Kowalczyk, T.; Krauter, C. M.; Lao, K. U.; Laurent, A. D.; Lawler, K. V.; Levchenko, S. V.; Lin, C. Y.; Liu, F.; Livshits, E.; Lochan, R. C.; Luenser, A.; Manohar, P.; Manzer, S. F.; Mao, S.-P.; Mardirossian, N.; Marenich, A. V.; Maurer, S. A.; Mayhall, N. J.; Neuscamman, E.; Oana, C. M.; Olivares-Amaya, R.; O'Neill, D. P.; Parkhill, J. A.; Perrine, T. M.; Peverati, R.; Prociuk, A.; Rehn, D. R.; Rosta, E.; Russ, N. J.; Sharada, S. M.; Sharma, S.; Small, D. W.; Sodt, A.; Stein, T.; Stück, D.; Su, Y.-C.; Thom, A. J. W.; Tsuchimochi, T.; Vanovschi, V.; Vogt, L.; Vydrov, O.; Wang, T.; Watson, M. A.; Wenzel, J.; White, A.; Williams, C. F.; Yang, J.; Yeganeh, S.; Yost, S. R.; You, Z.-Q.; Zhang, I. Y.; Zhang, X.; Zhao, Y.; Brooks, B. R.; Chan, G. K. L.; Chipman, D. M.; Cramer, C. J.; Goddard, W. A.; Gordon, M. S.; Hehre, W. J.; Klamt, A.; Schaefer, H. F.; Schmidt, M. W.; Sherrill, C. D.; Truhlar, D. G.; Warshel, A.; Xu, X.; Aspuru-Guzik, A.; Baer, R.; Bell, A. T.; Besley, N. A.; Chai, J.-D.; Dreuw, A.; Dunietz, B. D.; Furlani, T. R.; Gwaltney, S. R.; Hsu, C.-P.; Jung, Y.; Kong, J.; Lambrecht, D. S.; Liang, W.; Ochsenfeld, C.; Rassolov, V. A.; Slipchenko, L. V.; Subotnik, J. E.; Van Voorhis, T.; Herbert, J. M.; Krylov, A. I.; Gill, P. M. W.; Head-Gordon, M. Advances in Molecular Quantum Chemistry Contained in the Q-Chem 4 Program Package. *Mol. Phys.* **2015**, *113* (2), 184–215.

(38) Reed, A. E.; Weinstock, R. B.; Weinhold, F. Natural Population Analysis. *J. Chem. Phys.* **1985**, *83* (2), 735.

(39) Tsuzuki, S.; Uchimaru, T.; Tanabe, K. Intermolecular Interaction Potentials of Methane and Ethylene Dimers Calculated with the Møller–Plesset, Coupled Cluster and Density Functional Methods. *Chem. Phys. Lett.* **1998**, *287* (1–2), 202–208.

(40) Brozek, C. K.; Dincă, M. Ti3+-, V2+/3+-, Cr2+/3+-, Mn2+-, and Fe2+-Substituted MOF-5 and Redox Reactivity in Cr- and Fe-MOF-5. *J. Am. Chem. Soc.* **2013**, *135* (34), 12886–12891.

(41) Khaliullin, R. Z.; Bell, A. T.; Head-Gordon, M. Analysis of Charge Transfer Effects in Molecular Complexes Based on Absolutely Localized Molecular Orbitals. *J. Chem. Phys.* **2008**, *128* (18), 184112.

(42) Weigend, F.; Ahlrichs, R. Balanced Basis Sets of Split Valence, Triple Zeta Valence and Quadruple Zeta Valence Quality for H to Rn: Design and Assessment of Accuracy. *Phys. Chem. Chem. Phys.* **2005**, *7* (18), 3297–3305.

(43) Auerbach, S. M.; Henson, N. J.; Cheetham, A. K.; Metiu, H. I. Transport Theory for Cationic Zeolites: Diffusion of Benzene in Na-Y. *J. Phys. Chem.* **1995**, *99* (26), 10600–10608.

(44) Klein, H.; Fuess, H.; Schrimpf, G. Mobility of Aromatic Molecules in Zeolite NaY by Molecular Dynamics Simulation. *J. Phys. Chem.* **1996**, *100* (26), 11101–11112.

(45) Smit, B.; Maesen, T. L. M. Molecular Simulations of Zeolites: Adsorption, Diffusion, and Shape Selectivity. *Chem. Rev.* **2008**, *108* (10), 4125–4184.

(46) Lin, L.-C.; Kim, J.; Kong, X.; Scott, E.; McDonald, T. M.; Long, J. R.; Reimer, J. A.; Smit, B. Understanding CO2 Dynamics in Metal–Organic Frameworks with Open Metal Sites. *Angew. Chem. Int. Ed.* **2013**, *52* (16), 4410–4413.

(47) Wang, W. D.; Lucier, B. E. G.; Terskikh, V. V.; Wang, W.; Huang, Y. Wobbling and Hopping: Studying Dynamics of CO2 Adsorbed in Metal–

Organic Frameworks via 17O Solid-State NMR. *J. Phys. Chem. Lett.* **2014**, *5* (19), 3360–3365.

(48) Chen, S.; Lucier, B. E. G.; Boyle, P. D.; Huang, Y. Understanding The Fascinating Origins of CO2 Adsorption and Dynamics in MOFs. *Chem. Mater.* **2016**, *28* (16), 5829–5846.

(49) Tsivion, E.; Mason, J. A.; Gonzalez, M. I.; Long, J. R.; Head-Gordon, M. A Computational Study of CH4 Storage in Porous Framework Materials with Metalated Linkers: Connecting the Atomistic Character of CH4 Binding Sites to Usable Capacity. *Chem. Sci.* **2016**.

Table of Contents (TOC) and Abstract Graphics